ECS Journal of Solid State Science and Technology, **4** (9) N103-N110 (2015)

Structural and Luminescent Properties of (Y,Cu)-Codoped Zirconia Nanopowders

N. Korsunska,[a] M. Baran,[a] Yu. Polishchuk,[a] O. Kolomys,[a] T. Stara,[a] M. Kharchenko,[b] O. Gorban,[b] V. Strelchuk,[a] Ye. Venger,[a] V. Kladko,[a] and L. Khomenkova[a,z]

[a] *V.E. Lashkaryov Institute of Semiconductor Physics, NAS of Ukraine, Kyiv 03028, Ukraine*
[b] *O.O. Galkin Donetsk Institute for Physics and Engineering, NAS of Ukraine, Kyiv 03028, Ukraine*

The effect of both CuO content (1 and 8 mol%) and calcination temperature (T_c = 500–1000°C) on light emitting and structural properties of ZrO_2-Y_2O_3-CuO nanopowders was studied by photoluminescence (PL), X-ray diffraction (XRD) and Raman scattering methods. The samples, calcinated at T_c = 500–700°C, contain the tetragonal ZrO_2 phase predominantly. The increase of T_c results in its transformation to monoclinic one, and the phase transformation happens at higher temperature at higher Cu content. It is shown that the increase of T_c from 500 to 800°C results in the Cu incorporation into nanocrystals from the surface entities. This manifests itself in the shift of XRD and Raman peaks of tetragonal phase. The PL spectra demonstrate the presence of two main PL components peaked at about 540 nm and 630 nm in the most samples. The increase of T_c from 500 to 1000°C results in the non-monotonic variation of total PL intensity as well as in minor changes in PL spectra shape. The evolution of PL intensity is explained by both the increase of a crystallinity degree and the variation of the concentration of non-radiative recombination centres. The transformation of PL spectra shape is ascribed to the appearance of radiative Cu_{Zr} centres.

[DOI: 10.1149/2.0021509jss]

Manuscript submitted May 11, 2015; revised manuscript received July 6, 2015. Published July 23, 2015. This was Paper 1476 presented at the Chicago, Illinois, Meeting of the Society, May 24–28, 2015.

Zirconia nanopowders has attracted considerable attention because of its mechanical, electric, thermal and luminescent properties offering diverse applications such as catalysts, high temperature and corrosion resistant coatings, sensors, radiation detectors, biological labelling, etc.[1–5] Different emission bands can be observed in visible spectral range from pure and/or Y-stabilized ZrO_2 materials allowing an application of zirconia for white light emitting devices.[6–8]

In recent years, along with ZrO_2, Cu-doped ZrO_2 and Cu-doped Y-stabilized ZrO_2 composite have been intensively investigated[9–12] due to their excellent properties (such as environmental degradation, catalytic activity and tribologocal behavior). These latter were analyzed along with the structural characteristics and were found to be depended on Cu localization in composite, namely they were connected with Cu itself or its compounds placed on the crystallite surface. At the same time, it is known that copper can also exist in ZrO_2 as highly dispersed in substitution sites (Cu_{Zr}).[12]

For successful application of ZrO_2-based nanopowders, an achievement of the state of weakly bound single nanocrystals is one of the main problems. Among different approaches for nanopowders' production, microwave hydrothermal synthesis,[1] high-temperature solid state reaction (ceramic powders),[13] sol-gel technique,[12,14] spray-pyrolysis approach[15,16] and chemical co-precipitation method[10,17,18] were used. The latter is one of the most widespread methods due to low cost and opportunity for industrial production of powders with prescribed chemical composition. However, this method suffers from some disadvantages such as a wide size distribution of nanoparticles and high degree of their agglomeration. To overcome both problems a method was modified,[19,20] namely the high-energy actions (such as the using of pulse magnetic field or microwave treatment) were included in a drying stage of chemical precipitation technology.

Though the structural properties of Cu-doped composites were intensively investigated, their light emitting characteristics were not examined. At the same time, Cu incorporation can affect light emitting properties.

Room temperature photoluminescence (PL) spectra of pure or Y-doped ZrO_2 show either several overlapped emission bands or single featureless broad band, whose the intensity and peak positions depend on excitation light wavelength, crystallite size, dopants and preparation technique.[6–8,21–25] This PL emission originates from defect states caused by the different structural defects[6–8,22] that can explain a variety of observed PL bands. These latter are attributed usually to intrinsic defects such as oxygen vacancies[26] or their complexes located in the crystal volume,[6,27] at grain surface[7] or near impurities.[6] In addition, T-defect (Zr^{3+} neighboring with two oxygen vacancies located in the crystal volume[28,29]) or unsaturated Zr sites at the crystal surface (surface Zr^{3+} centers[30]) as well as the lattice distortion by oxygen vacancies[8] were considered as PL sources. The shift of PL peak position with the variation of the excitation light wavelength[6,8,17] is obviously caused by the overlapping of different PL bands.

It is known that an introduction of impurities with the valence lower than valence of Zr results in the stabilization of the tetragonal or cubic phase of ZrO_2 and formation of oxygen vacancies. This can result in the increase of the intensity of the PL bands related to these vacancies or their complexes with the impurity. Such an effect was observed in[7] where the intensities of the PL bands peaked at 450 nm and 570 nm increased with the increase of Y content. Based on linear dependence of the intensity of the 450-nm PL band on the Y content this emission was ascribed to bulk vacancies which appearance is stimulated by Y ions.[7] At the same time, the 570-nm PL band, whose dependence on Y content deviated from linear relationship, was associated with localized states at the grain boundaries or at the grain surface. It was shown,[31,32] that Cu incorporation in ZrO_2 also results in stabilization of tetragonal and cubic phase. Therefore, it can be expected that doping of ZrO_2 with Cu can also enhance the PL band resulted from oxygen vacancies. On the other hand, the appearance of additional Cu-related band can also give the contribution to PL spectra. Generally, this band can be caused by intra-defect transition in Cu ions or radiative capture of free carriers by Cu-related centers as well as originates from complexes of oxygen vacancies with Cu ions. Specifically, green PL band, conditioned by intra-defect transition in Cu impurity[33] or free electron capture by Cu^{2+} ions, was observed in wide bandgap compounds.[34] Thus, it can be expected that PL study can give information on Cu spatial localization in composite. On the other hand, an achievement of Cu-related green emission in ZrO_2-based composites could allow considering of this materials as a green light source.

In present work the interrelation of light emitting and structural properties of the ZrO_2-Y_2O_3-CuO nanopowders produced by

---

[z] E-mail: khomen@ukr.net

microwave-assisted co-precipitation method were investigated versus Cu content and calcination temperature by means of XRD, Raman scattering and PL methods.

Experimental

The Y-stabilized ZrO_2 nanopowders doped with Cu were synthesized by a co-precipitation technique using Zr, Y and Cu nitrates in molar ratio $ZrO(NO_3)_2$:$Y(NO_3)_3$:$Cu(NO_3)_2$ = 96:3:1 or 89:3:8 in distilled water. With such a composition the CuO concentration of 1 mol% (Cu-1) or 8 mol% (Cu-8) was obtained, whereas the Y_2O_3 content was fixed at 3 mol% for both sets.

The 6 wt% ammonia solution was used for a chemical precipitation. This latter was carried out at pH = 10–11 followed by precipitate washing to pH = 7. After washing with distilled water and filtering, the microwave irradiation with a power of 700 Wt and a frequency of 2.45 GHz was used for the synthesis of the amorphous xerogel nanopowders from hydrogel. Then the xerogel nanopowders were calcined at T_c = 500–1000°B for 2 h. The powders were pressed in the pellets of 8 mm in diameter and 6 mm in thickness (so called as the Cu-1 or Cu-8 samples).

Structural, optical and light emitting properties were studied by X-ray diffraction (XRD), micro-Raman scattering, electron paramagnetic resonance (EPR), PL and PL excitation methods at room temperature. XRD data were collected in the range of $2\theta = 20–80°$ using Thermo Scientific ARL X'TRA diffractometer with $Cu_{K\alpha}$ wavelength ($\lambda = 0.15418$ nm) in Bragg geometry. The Raman scattering spectra of all samples were acquired in a quasi-backscattering geometry using the Horiba Jobin-Yvon T64000 spectrometer integrated micro-Raman setup with Olympus BX-41 microscope and air-cooled CCD detector. The 100× and 50× objectives were used to focus the laser beam and to collect the back-scattered light, respectively. The spectral resolution was about 0.3 cm^{-1}. The experiments were carried out using the 488.0 nm line of an Ar/Kr laser. EPR spectra were measured using Varian-12 spectrometer. The modulation frequency was 100 kHz and modulation amplitude was 0.1–0.2 mT. Photoluminescence was excited with the light of Xe lamp dispersed by grating monochromator. PL spectra were registered in the range 450–900 nm using monochromator IKS-12 and photomultiplier.

Results

Structural properties.—XRD data.—Typical undoped ZrO_2 powders with monoclinic and tetragonal structures demonstrate several XRD reflections in the range of $2\theta = 25–55°$. For the monoclinic phase the peaks are observed at 28.05° (11-1), 31.33° (111), 33.98° (002), 34.25° (020), 35.15° (200), 35.71° (10-2), 49.02° (022), 49.89° (220), 50.31° (12-2) and 53.84° (202). These peaks were indexed corresponding to JCPDS 37–1484. For tetragonal phase the peaks at $2\theta \sim 30.4°$, 35.5°, 50.5° correspond to (111), (002) and (220) reflections (JCPDS 80–0784).

As one can see from Fig. 1a, XRD patterns for the Cu-1 and Cu-8 samples calcined at T_c = 500°C represent mainly tetragonal ZrO_2 phase (curves 1, 2). This phase dominates up to T_c = 800°C in both types of the samples. Besides, the XRD peak positions corresponded to this phase in the Cu-8 samples are shifted to higher angles in comparison with those in the Cu-1 samples.

For the Cu-1 samples an appearance of monoclinic phase at low amount (~1-2%) is observed after calcination at T_c = 700 and 800°C (Table I). Higher T_c results in the sharp increase of this phase contribution up to 70% for T_c = 1000°C. At the same time in the Cu-8 samples the monoclinic phase (curve 3) appears at T_c = 900°C and further increase of T_c up to 1000°C results in the rise of its contribution up to 55% (Table I). Besides the phase transformation, the shift of XRD peaks corresponded to tetragonal phase toward higher angles with the increase of T_c is observed. This shifting occurs up to the T_c values corresponded to the phase transformation in both types of the samples (Fig. 1b). However, the shift value in the Cu-1 samples is lower than in the Cu-8 samples.

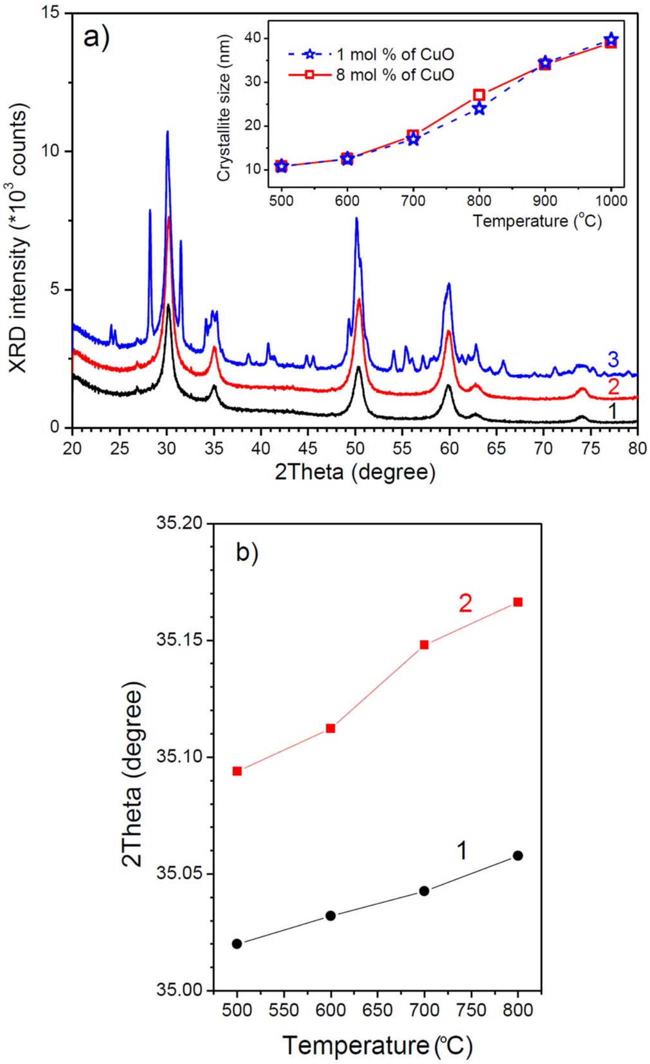

Figure 1. a) XRD patterns of Cu-1 (1) and Cu-8 (2,3) samples calcined at 500°C (1,2) and 1000°C (3). Inset – the variation of tetragonal crystallite sizes with T_c. b) The shift of (002) XRD peak of tetragonal phase for the Cu-1 (1) and Cu-8 (2) versus T_c.

The coherent domain sizes of tetragonal phase, *d*, (crystallite mean size) were estimated from XRD data using Scherrer formula $d = K\lambda/(\beta \cdot \cos\theta)$, where K = 0.9 is a dimensionless shape factor, $\lambda = 0.15418$ nm, β is a full width at half the maximum intensity (FWHM); θ is the Bragg angle. The *d* values were found to increase gradually from 10.8 nm (500°C) up to 40 nm (1000°C) being independent practically on CuO content (Fig. 1, insert, Table I).

Raman scattering spectra.—The Raman spectra of the Cu-1 and Cu-8 samples calcined at different temperatures are shown in Figs. 2a,2b. When the Cu-1 sample was calcinated at T_c = 500°C, the Raman spectrum showed six major bands (Fig. 2a), which were the characteristic bands of ZrO_2 tetragonal phase. Among them the broad bands peaked at about 148, 472 and 637 cm^{-1} are attributed to E_g modes, the peak at about 269 cm^{-1} corresponds to A_{1g} mode and broad peaks at 322 and 607 cm^{-1} are related to B_{1g} modes. The peak positions in our samples slightly differ from mentioned above values that can be caused by powder compacting in pallets and by the doping.

After calcination at T_c = 700 and 800°C additional two small Raman peaks corresponded to monoclinic ZrO_2 phase appear at 178 and 190 cm^{-1} (A_g-bands). The increase of T_c up to 900°C results in

Table I. Phase composition and coherent domain size in Cu-1 and Cu-8 samples calcinated at different temperatures.

	Cu-1		Cu-8	
Calcination temperature, °C	Phase content, %	Coherent domain size, nm	Phase content, %	Coherent domain size, nm
500	100 (T)	10,8	100T	10,8
600	100T	12,5	100T	12,5
700	1M-99T	17	100T	17,8
800	1M-99T	26,5	100T	27
900	23M-77T	34,4 (T)	19M-81T	34 (T)
1000	70M-30T	40 (T)	55M-45T	39 (T)

the rise of the set of A_g modes (peaked at 178, 190, 303, 346, 474, 558 and 637 cm^{-1}) and B_g modes (peaked at 221, 333, 380, 502, 535 and 614 cm^{-1}) corresponded to monoclinic ZrO_2 phase. Besides, the A_{1g} peak and low frequency E_g peak from tetragonal ZrO_2 phase which are not overlapped with the peaks from monoclinic one are still observed.

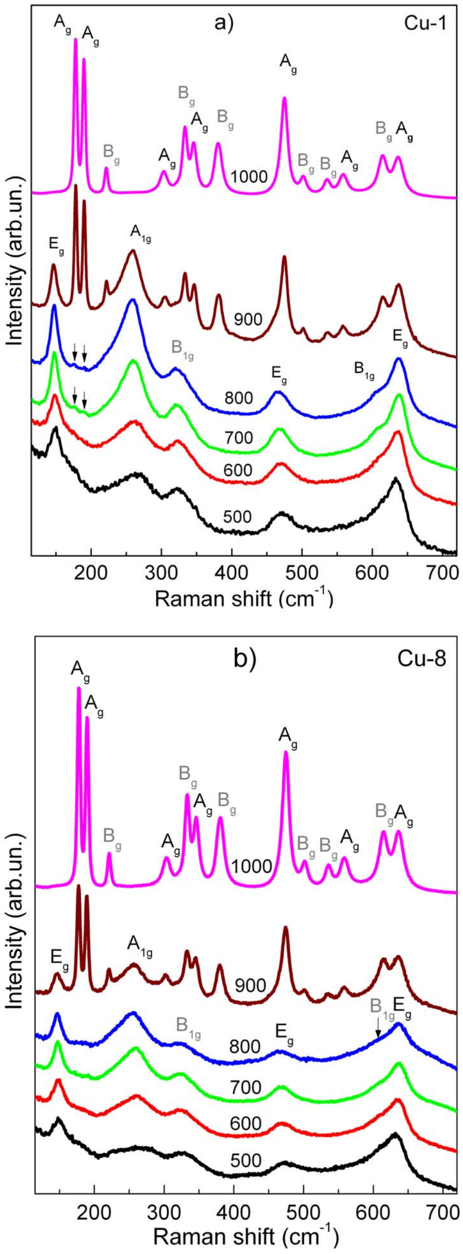

Figure 2. Raman scattering spectra of the Cu-1 (a) and Cu-8 (b) samples calcintated at 500–1000°C.

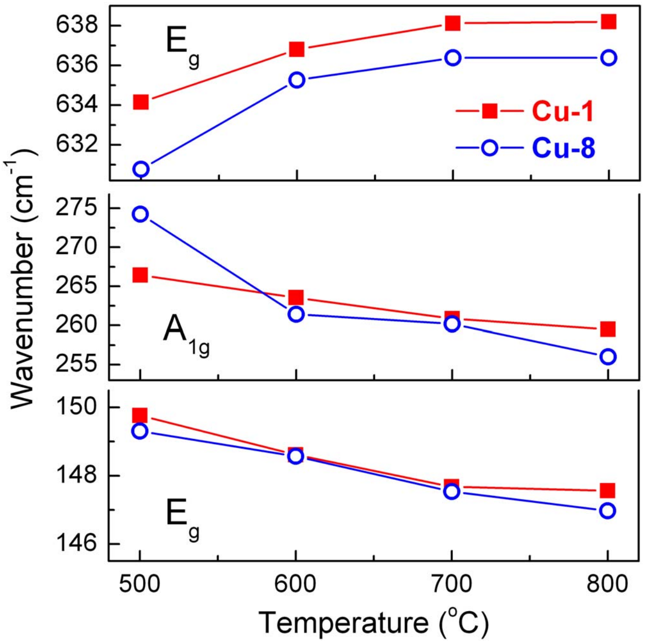

Figure 3. The frequency shift of Raman peaks versus calcination temperature of the Cu-1 (squares) and Cu-8 (circles) samples.

The Raman spectrum of the Cu-1 sample calcinated at 1000°C demonstrates the peaks of monoclinic ZrO_2 phase only. At the same time, the peaks from tetragonal ZrO_2 phase, in contrast to XRD data, were not clearly observed. This can be explained by a large difference in Raman scattering cross sections between the tetragonal and monoclinic ZrO_2 phases.

As one can see from Fig. 2b, for the Cu-8 samples calcinated at $T_c = 500–800$°C the Raman spectra show only the peaks from tetragonal ZrO_2 phase. The peaks from monoclinic phase appear at $T_c = 900$°C and the calcination at 1000°C similarly to the Cu-1 samples results in the presence of these peaks only.

It should be noted that for the Cu-8 samples all Raman peaks of tetragonal ZrO_2 phase are wider than the peaks of the Cu-1 ones. As temperature increases, the width of Raman peaks in the Cu-1 samples decreases while in the Cu-8 samples such an effect is not clearly observed. An exception is the behavior of the peak at about 270 cm^{-1} in the temperature interval of 500–600°C.

Besides the phase transformation, the shift of Raman peaks corresponded to tetragonal ZrO_2 phase occurs with the T_c increase. Figure 3 shows the dependence of the spectral positions of more intense tetragonal Raman peaks on calcination temperature for Cu-1 and Cu-8 samples. It is seen that both A_{1g} peak at about 270 cm^{-1} and E_g peak at about 148 cm^{-1} shift to low energy side while the E_g peak at about 633 cm^{-1} shifts to higher frequencies. The shift value especially for

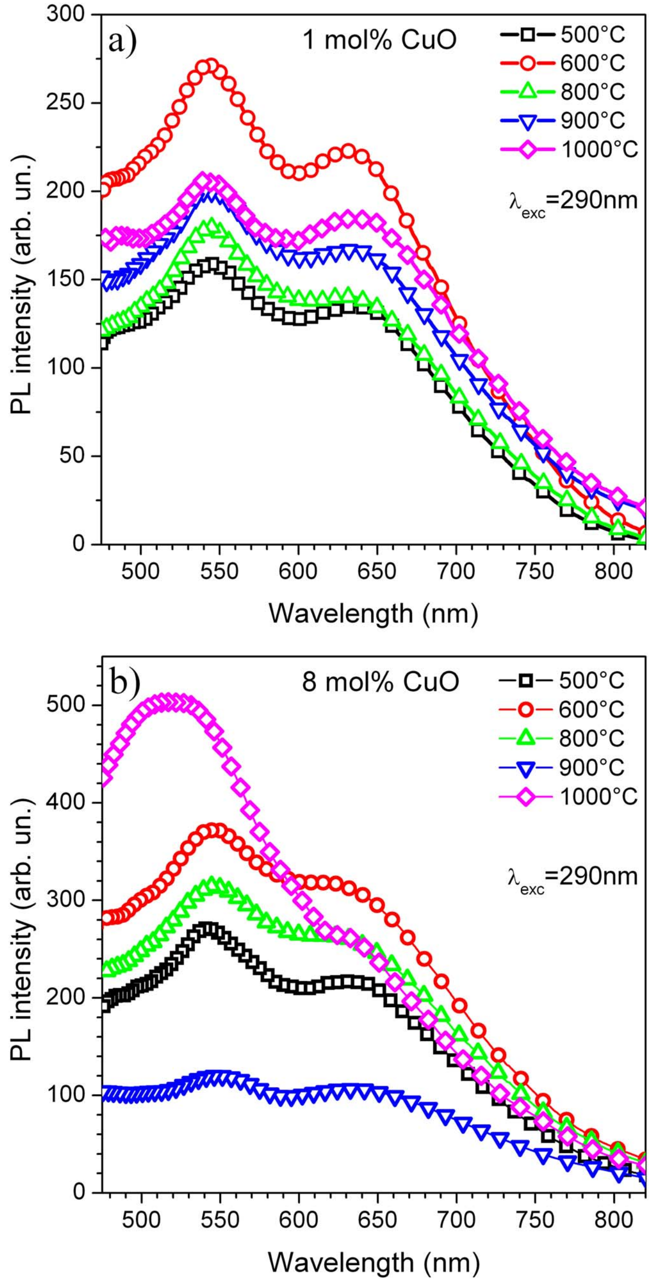

Figure 4. PL spectra of the samples with 1 mol% (a) and 8 mol% (b) of CuO calcined at $T_c = 500–1000°C$. The PL spectra for the samples calcinated at $T_c = 700°C$ are not shown since they are very close to those for the samples calcinated at $T_c = 500°C$.

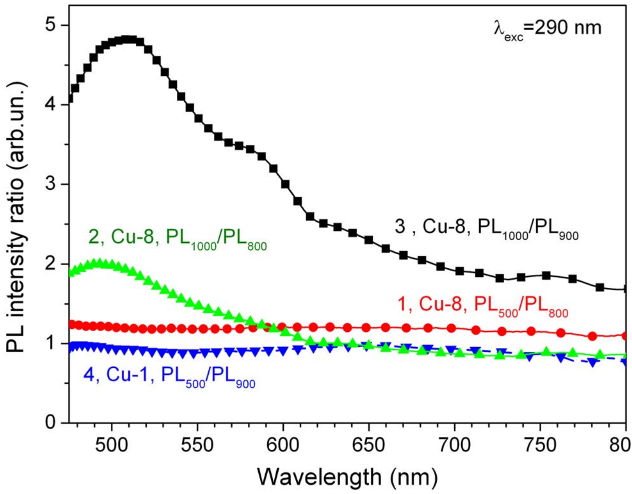

Figure 5. The ratio of PL spectra of the Cu-8 (1-3) and Cu-1 (4) samples calcinated at different temperatures. The curves represent the result of division of PL spectrum of Cu-8-500°C to that of Cu-8-800°C (1), of PL spectrum of Cu-8-1000°C to Cu-8-800°C (2) and of PL spectrum of Cu-8-1000°C to Cu-8-900°C (3) as well as of PL spectrum of Cu-1-500°C sample to that of Cu-1-900°C one (4).

A_{1g} peak and E_g peak at 633 cm^{-1} is higher for the Cu-8 samples as compared to that for the Cu-1 samples (Fig. 3).

Light emitting properties of the samples.— Photoluminescence spectra of the (Cu,Y)-ZrO_2 samples with different Cu content excited with 290-nm light wavelength are presented in Figs. 4a,4b. In the samples calcinated at 500–800°C they contain two broad emission bands with maxima at ∼540 nm ("green" PL) and ∼630 nm ("orange" PL) as well as the long-wavelength tail extended up to 900 nm. The intensity of "green" PL band is slightly higher than that of "orange" one.

At the same time the sample calcination at 900–1000°C results in the change of PL spectra shape. Specifically, in the Cu-8 samples calcinated at $T_c = 1000°C$ the broadening of "green" band and the formation of a plateau near its maximum is observed (Fig. 4b). This transformation is obviously caused by the appearance of additional green PL component. In the Cu-1 samples calcination at 1000°C results in the increase of the PL intensity in the 470–500 nm spectral range (Fig. 4a).

To trace the influence of calcination temperature on PL spectra shape we used the ratio of PL spectra of the samples calcinated at different temperatures.

Figure 5 shows that the ratio of PL spectrum of the Cu-8 sample calcinated at 800°C to PL spectrum of the sample calcinated at 500°C is constant in whole spectral range (curve 1). Nearly the same result is observed for the any two PL spectra selected in the interval 500°C–800°C (not shown). This demonstrates the independence of PL spectra shape on T_c in this T_c interval. At the same time the ratio of PL spectrum of the Cu-8 sample calcinated at $T_c = 1000°C$ to PL spectrum of the sample calcinated at $T_c = 800°C$ shows the broad maximum at ∼480 nm (Fig. 5, curve 2). This testifies to the dominant increase of PL intensity in the blue-green spectral range in the former sample. The ratio of PL spectra of the samples calcinated at $T_c = 1000°C$ and 900°C represents two maxima at ∼510 nm and ∼580 nm (Fig. 5, curve 3) which indicate the appearance or enhancement of the corresponded PL bands in the sample calcinated at $T_c = 1000°C$. Thus, it can be concluded that the additional green PL component, appeared at $T_c = 1000°C$ in the Cu-8 sample, is located near 510 nm. For the Cu-1 samples the shape of PL spectra does not change in the interval of $T_c = 500–900°C$ giving the constant ratio (Fig. 5, curve 4). At the same time for the sample calcinated at $T_c = 1000°C$ a slight increase of PL intensity is observed in 470–480 nm spectral range only (Fig. 4a).

PL excitation spectra (PLE) were found to be similar for main PL bands and contain the broad maximum near 280–290 nm (4.42–4.28 eV) (Fig. 6a). At the same time the shape of PL spectra varies with excitation light wavelength (Fig. 6b). This means that they consist of several overlapping components that is typical for pure and Y-doped ZrO_2 materials.[8,17,25] and the references therein On the other hand, this variation implies that besides the common intense excitation at ∼280 nm, PL bands possess the individual excitation features. Unfortunately, these latter cannot be clearly separated due to significant overlapping of PL bands. However, the variation of excitation wavelength allows determining the spectral range in which the different PL bands can be seen separately (Fig. 6b).

It should be noted that the 280–290 nm excitation band is usually ascribed to self-trapped exciton[5] which can participate in the excitation

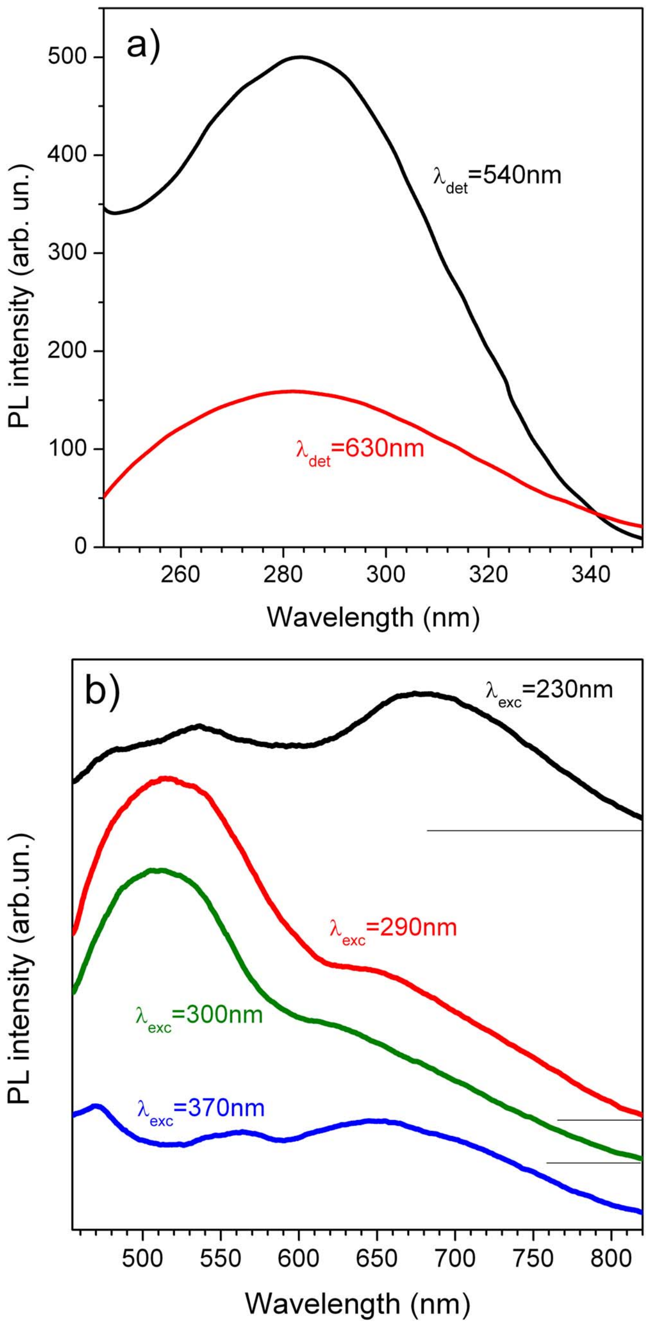

Figure 6. Luminescent characteristics of the Cu-8 sample calcinated at 1000°C: a) PLE spectra detected at 540 nm and 630 nm; b) PL spectra excited with 230, 290, 300 and 370-nm light wavelength.

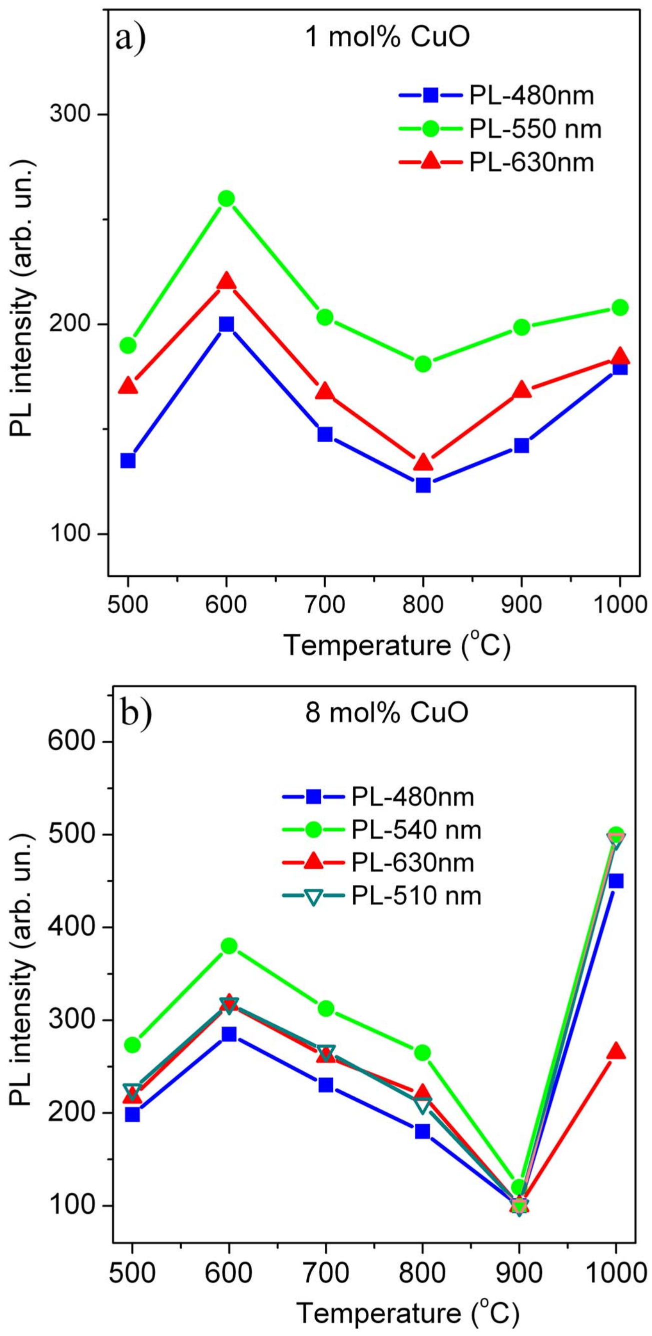

Figure 7. Variation of the intensities of different PL bands on calcination temperature for the Cu-1 (a) and Cu-8 (b) samples.

of different PL bands. At the same time the emission centers often have the individual excitation bands. They can correspond either to carrier transition from the ground to excited states of the centers (intradefect transitions), the bound excitons or the carrier excitation from the defect level to permitted band.

The intensities of all PL components depend essentially on calcination temperature and Cu content (Fig. 7). For the Cu-1 samples the dependences for the 480-nm, 540-nm and 630-nm PL components are shown in Fig. 7a. Besides these PL bands, for the Cu-8 samples Fig. 7b shows the evolution of the PL intensity at about 510 nm because this PL component appears clearly after high temperature calcination.

As one can see, the increase of calcination temperature leads to non-monotonous behavior of PL intensity. At first, when T_c increases from 500°C to 600°C, PL intensity of all components increases. Then it gradualy decreases up to $T_c = 800$°C for the Cu-1 samples and 900°C for the Cu-8 ones. Futher T_c rise results in PL intensity increase for both sample sets. It is interesting that such a variation of PL intensity is more pronounced for the Cu-8 samples (Fig. 7b). It should be noted that for the Cu-8 sample calcinated at $T_c = 1000$°C the PL intensities of both "green" bands increase sharper than that of 540-nm PL band for the Cu-1 sample.

Discussion

Structural properties.— As XRD data show the increase of calcination temperature results in the increase of the crystallite sizes and the transformation of tetragonal phase into monoclinic one (*t-m* transition). The latter depends on CuO content. Its increase leads to the

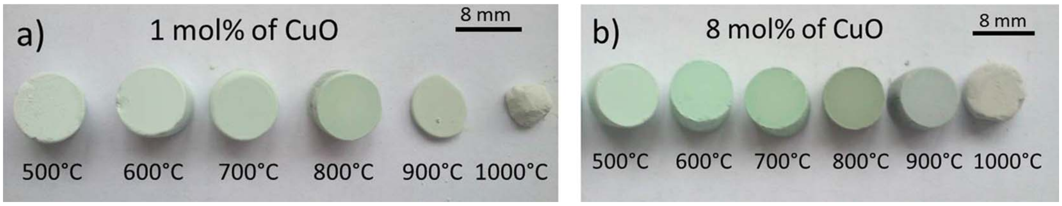

Figure 8. Evolution of the color of the Cu-1 (a) and Cu-8 (b) samples with calcination temperature.

shift of this transition to the higher temperature and the decrease of monoclinic phase contribution. This argues that Cu incorporated into ZrO_2-Y_2O_3 matrix promotes the stabilization of tetragonal phase that is in agreement with data obtained by other authors[11] and with our Raman scattering data. In fact, the peaks corresponded to monoclinic phase in Raman scattering spectra of the Cu-1 samples appear at lower calcination temperature than in the spectra of the Cu-8 samples.

The shift of the XRD peaks corresponded to tetragonal phase with the increase of T_c (up to the temperature when monoclinic phase appears) indicates the decrease of lattice constant. The increase of shift value with CuO content allows assuming that Cu incorporation is the reason of this effect. This is in agreement with the data of Ref. 11 Therefore, it can be concluded that the T_c increase results in the copper enrichment of nanocrystallites due to Cu diffusion from surface entities. At the same time, the shift of tetragonal XRD peaks of the Cu-8 samples in comparison to that of the Cu-1 sample for all T_c values toward the higher angles testifies to the higher Cu content in the Cu-8 samples and means that Cu incorporation into nanocrystals occurs at 500°C already.

The shift of XRD peak positions with the increase of calcination temperature is in agreement with Raman scattering data. In fact, the Raman peaks, corresponded to tetragonal phase, also shift when temperature increases from 500 to 800°C. Because the shift value rises with the increase of CuO content (Fig. 3), we can conclude that this effect is caused by Cu incorporation in the ZrO_2-Y_2O_3 matrix. The shift of the A_{1g} peak to the low energy side and of the E_g peak (at about 633 cm^{-1}) to the high energy side were observed in tetragonal ZrO_2 under hydrostatic pressure.[16] Therefore, we can assume that the compressive stresses increase with calcination temperature that is in agreement with the decrease of the lattice constant supported by the XRD data. However, the behavior of another E_g peak (at 148 cm^{-1}) differs from it behavior under hydrostatic pressure. This can be assigned to the change of the tetragonality ratio (*c/a*) that is in agreement with XRD data.[11] Thus, the shift of Raman peaks with the increse of calcination temperature in the range $T_c = 500$–800°C confirms the increase of Cu content in the nanocrystallites.

It should be noted that Raman scattering spectra can give additional information on structural characteristic of the samples investigated. In fact, another feature of Raman spectra transformation with the T_c rise is the narrowing of Raman peaks observed for the Cu-1 samples at T_c = 500–900°C. Similar effect for the Cu-8 samples was observed for T_c = 500–600°C only, being more pronounced than in Cu-1 samples.

Generally, such narrowing can be caused by several reasons: i) by the increase of crystallinity degree, ii) decrease of defect number or iii) by quantum confinement effect. The latter is not realized in our samples because the narrowing of the Raman peaks at $T_c > 600$°C is observed in the Cu-1 samples only in spite of the similar crystallite sizes in both types of the samples (Fig. 1a, inset). At the same time, the decrease of Raman peak width with T_c increase from 500 to 600°C can be caused by the increase of crystallinity degree. In this case, the broader Raman peaks at $T_c = 500$°C and their more pronounced narrowing at $T_c = 500$–600°C in the Cu-8 samples can be explained by the shift of the crystallization process to the higher temperatures due to the inhibition of this process by copper. Such an effect was earlier observed for ZrO_2-Y_2O_3 powders doped with Cr.[18] The measurements of crystallization temperatures for our samples also confirm this assumption. The sharp increase of crystallinity degree takes place at T = 440°C (for ZrO_2-Y_2O_3), 455°C (for ZrO_2-Y_2O_3-CuO with 1 mol% of CuO) and 485°C (for ZrO_2-Y_2O_3-CuO with 8 mol% CuO). At the same time, the peak narrowing in the Cu-1 samples at higher temperatures is obviously caused by the decrease of defect number, including the defects at the crystallite surface.

One more feature of Raman spectra is the higher value of peak width in the Cu-8 samples as compared to the Cu-1 samples, which is observed not only at low but also at high calcination temperatures when crystallization process is completed. This fact and the absence of temperature-stimulated narrowing effect in the Cu-8 samples for $T_c > 600$°C can be explained by the higher defect density in these samples caused by the higher Cu content in the crystallites. In fact, the Cu incorporation, resulting in the stabilization of tetragonal phase, is accompanied by oxygen vacancies formation.[31]

The Cu incorporation into the samples is confirmed also by the coloration of samples investigated. In fact, they have greenish color (Fig. 8). Its intensity increases with Cu content and depends on calcination temperature. With its increase the color changes: the green color at first enhances, whereas after appearance of monoclinic phase, the color becomes grey-like. Because the substances, which can be present on the crystallite surface (CuO, Cu_2O, yttrium cuprate), cannot give such a coloration, it can be assigned to color centers. It is known that the Cu ions have the absorption band in green spectral range[35] and can be responsible for the greenish coloration. Thus, its enhancement testifies to Cu incorporation into the nanocrystals. The decrease of greenish coloration after calcination at 900 and 1000°C can be caused by the decrease of the Cu_{Zr} content in the crystallites.

Light emitting properties.— The Cu incorporation influences also the PL properties. This becomes apparent in the dependence of PL intensities and spectra shape on calcination temperature. As the results described above show, one of the main features of PL characteristic is the non-monotonic variation of PL intensity with calcination temperature. The increase of PL intensity of all bands in the temperature range of 500–600°C, which correlates with the narrowing of Raman peaks, can be explained by the increase of crystallinity degree. Weaker increase of PL intensity, observed for the Cu-8 samples in comparison to that for the Cu-1 ones, also correlates with the different narrowing of Raman peaks in these samples. This is in agreement with the above-mentioned supposition that Cu can hamper the crystallization process.

Further increase of T_c up to temperatures, resulting in monoclinic phase formation, leads to the quenching of all PL bands without of the change of PL spectra shape. This allows concluding that this effect is caused by appearance of fast non-radiative recombination centers. In this case the proportional decrease of all bands intensity can be expected. Generally, such centers can be located at the crystallites' surface or in their volume. The evolution of crystallite sizes with T_c shows that the PL intensity decreases when the crystallite sizes increase. The latter leads to the decrease of surface/volume ratio and has to result in the decrease of surface role in recombination processes. Therefore, we can conclude that non-radiative channel is located in the volume of the crystallites. Because the degree of PL quenching increases with the CuO content, we can assume that appearance of these centers is caused by Cu incorporation in ZrO_2-Y_2O_3 matrix. As it was mentioned above, this process results in the stabilization of tetragonal phase and leads to the formation of oxygen vacancies and Zr^{3+} centers. As it was shown earlier,[25] the Zr^{3+} surface defect is the fast recombination center. This allows assuming that Zr^{3+} center in the crystal volume can also serve as non-radiative center which results in the decrease of PL intensity. Thus, the main effect caused by Cu incorporation is total PL quenching contrary to the result of Y incorporation described in Ref. 7 which shows the increase of the intensities of certain PL bands. This can be caused by the higher defect density stimulated by Cu incorporation into ZrO_2 (including the non-radiative centers) due to higher difference in the valences of Zr and Cu atoms.

The subsequent increase of the PL intensity correlates with the appearance of monoclinic phase, where the number of oxygen vacancies (and correspondingly Zr^{3+} centers) decreases. This confirms that the non-radiative centers are the native defects.

It should be noted that the increase and the decrease of PL intensity (the contribution of nonradiative recombination channel) correlate with the increase and the decrease of coloration degree. Because the number of vacancies and Zr^{3+} defects depend on Cu content, this is apparently the reason of the interrelation of PL intensity and sample color. The appearance of intrinsic non-radiative defects can be also the reason of lower PL intensity of tetragonal phase in comparison with that of monoclinic one that was observed by us earlier for ZrO_2 nanopowders doped with Y only.

Besides the PL intensity variation, it was also observed the changes in PL spectra shape, i.e. the appearance or the increase in intensity of certain PL bands. Specifically, in the Cu-1 samples it is the blue band, while in Cu-8 samples it is new green band at ∼510 nm. The latter is evidently the reason of sharper PL intensity rise observed under 290-nm light excitation in the Cu-8 samples comparing to the Cu-1 ones. The blue band is usually observed in ZrO_2 with different Y_2O_3 content and ascribed to oxygen vacancies, while the green band can be attributed to Cu ions incorporated into nanocrystals. The interrelation of the green band with Cu ions is confirmed by its observation in the sample with higher Cu content. Besides, this interrelation is verified also by the following experiment.

The Cu-8 sample calcined at 1000°C was submitted to an additional annealing at 1100°C for 20 min followed by a quenching (for several minutes down to room temperature). The EPR and PL spectra before and after this treatment were compared. Before additional annealing the EPR spectrum showed the signal consisted of several narrow lines and could be assigned to Cu^{2+} centers in lattice sites (Fig. 9a, curve 1). After annealing the intensity of this signal decreased and another broad Cu-related EPR signal appeared (Fig. 9a, curve 2). Similar broad signal was observed for the samples calcinated at $T_c = 500–700°C$ (curve 3). Its intensity reduced with the T_c rise, when the Cu content increased in nanocrystal volume due to Cu diffusion from its surface. Thus, this EPR signal originates from the Cu-related surface entities. The similar broad signal was observed in Cu-doped TiO_2,[36] nonstoichiometric CuO,[37] Cu contained glasses[38] or solutions.[39] In Ref. 36 this signal was ascribed to Cu-related surface complexes. It was shown that in this case the parameters of EPR signal (g-factor, hyperfine coupling and anisotropy) depend on the structure of complex and the type of ligands.[36,39] The formation of surface complexes or CuO is supported by the appearance of the Raman peak at $\sim 280\ cm^{-1}$ (not shown) that could be related to CuO[40] or cuprates. Such transformations of EPR and Raman scattering spectra can be explained by the outward diffusion of Cu atoms from nanocrystal volume to its surface. It should be noted that the annealing at 1100°C followed by slow cooling (for 3 hours) does not result in the appearance of broad EPR signal and the Raman peak at $\sim 280\ cm^{-1}$. This fact can be explained by sufficient time for the Cu atoms to be returned into the nanocrystal volume and it supports our conclusion about Cu outdiffusion upon additional annealing followed by fast quenching.

It is essentially that the latter treatment resulted in the decrease of total PL itntensity, but the intensity of green PL band peaked at 510 nm reduced mainly (Fig. 9b) that testified to its relation with Cu^{2+} ions at lattice sites. As it was mentioned, similar Cu-related PL emission (500–530 nm) was observed in other wide bandgap compounds[33,35] and in some cases it was attributed to the intradefect transition in the Cu^{2+} ions.[35] It was shown that this emission can be excited via light absorption by Cu^{+} ions. In our case, the green emission can be excited both by self-trapped exciton (280–290-nm) and, possibly, by the bound exciton (300–310 nm).

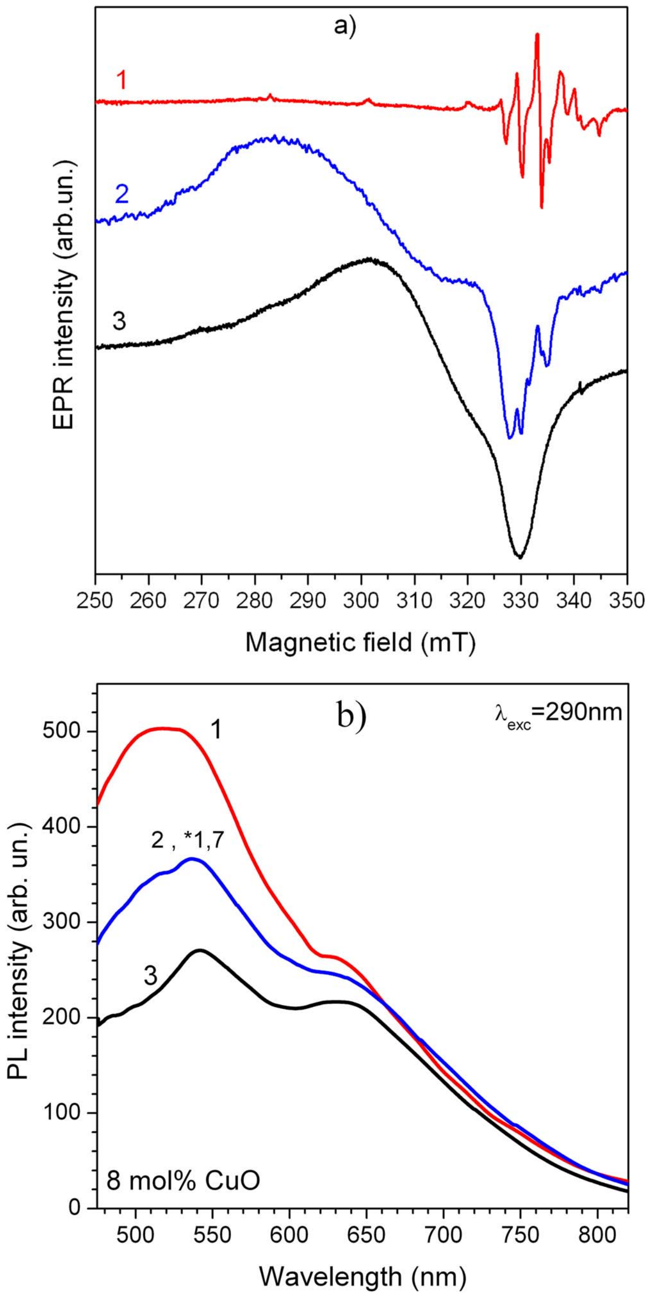

Figure 9. EPR(a) and PL (b) spectra of the Cu-8 samples calcined at 1000°C (1) and after its annealing at 1100°C for 20 min followed by quenching (2). Curves (3) correspond to EPR (a) and PL (b) spectra of Cu-8 sample calcinated at 500°C.

Thus, Cu incorporation into the nanocrystals can result in not only the enhancement of non-radiative channel but also the appearance of specific PL band caused, probably, by intradefect radiative transition in Cu_{Zr} centers.

Conclusions

The effect of calcination temperature and Cu content on the photoluminescence spectra and structural properties of ZrO_2-Y_2O_3-CuO samples was investigated. XRD and Raman scattering spectra show that the samples, calcinated at low temperatures, contain the tetragonal phase predominantly. The temperature increase stimulates the transformation of tetragonal phase to monoclinic one. The higher Cu content results in the higher temperature of phase transformation. The increase of T_c from 500 to 800°C leads to the shift of XRD and Raman peaks from tetragonal phase. This shift corresponds to the increase of compressive stress testifying to the Cu incorporation in the crystallites with T_c increase. The PL spectra of the most samples show the presence of two main PL components peaked at about 630 nm and 540 nm. The change of calcination temperature in the 500–1000°C range results in the non-monotonic variation of total PL intensity as well as in the minor changes in PL spectra. The increase of calcination temperature from 500 to 600°C leads to the increase of total PL intensity, which can be ascribed to the increase of crystallinity degree. The further PL intensity decrease with temperature increase (up to 800–900°C) is caused by the appearance of non-radiative recombination centers in the crystallite volume conditioned by the formation of intrinsic defects (probably, Zr^{3+}) due to Cu incorporation. The consequent enhancement of PL intensity correlates with phase transformation from tetragonal to monoclinic and can be explained by the decrease of the concentration of these centres in monoclinic phase. The calcination of the sample with 8mol% of CuO at high temperatures results also in the appearance of additional green PL band, which can be assigned to Cu_{Zr} centres.

Acknowledgments

This work was supported by National Academy of Sciences of Ukraine (project III-4-1).

References

1. J. D. Fidelus, W. Łojkowski, D. Millers, L. Grigorjeva, K. Smits, and R. R. Piticescu, *Sol. St. Phenom.*, **128**, 141 (2007).
2. J. D. Fidelus, W. Lojkowski, D. Millers, K. Smits, and L. Grigorjeva, *IEEE Sensors*, **9**, 1268 (2009).
3. H. Ken Yueh and B. Cox, *J. Nucl. Mat.*, **323**, 57 (2003).
4. R. Jia, W. Yang, Y. Bai, and T. Li, *Opt. Mater.*, **28**, 246 (2004).
5. M. Kirm, J. Aarik, M. Jurgens, and I. Sildos, *Nucl. Insrtum. Methods Phys. Res. A*, **537**, 251 (2005).
6. N. G. Petrik, D. P. Tailor, and T. M. Orlando, *J. Appl. Phys.*, **85**, 6770 (1999).
7. H. Nakajima and T. Mori, *J. Alloys Compound.*, **408–412**, 728 (2006).
8. K. Smits, L. Grigorjeva, D. Millers, A. Sarakovskis, J. Grabis, and W. Lojloeski, *J. Lumin.*, **131**, 2058 (2011).
9. L. Kong, Q. Bi, Sh. Zhu, Zh. Qiao, J. Yang, and W. Liu, *J. Europian Ceram. Soc.*, **34**, 1289 (2014).
10. L. Winnubst, Sh. Ran, E. A. Speets, and D. H. A. Blank, *J. Europian Ceram. Soc.*, **29**, 2549 (2009).
11. Y. Sh. Zhang, L. T. Hu, H. Zhang, J. M. Chen, and W. M. Liu, *J. of Mat. Proc. Technol.*, **198**, 191 (2008).
12. Y. Sun and P. A. Sermon, *Catalist Letters*, **29**, 361 (1994).
13. N. L. Shukla, S. V. Sharma, P. Chand, and B. N. Misra, *Acta Phys. Polon. A*, **83**, 441 (1993).
14. X. Tang and X. Zheng, *J. Mater. Sci. Technol.*, **20**, 485 (2004).
15. E. Djurado and E. Meunier, *J. Solid State Chem.*, **140**, 191 (1998).
16. P. Bouvier and G. Lucazeau, *J. Phys. Chem. Sol.*, **61**, 569 (2000).
17. N. Korsunska, V. Papusha, O. Kolomys, V. Strelchuk, A. Kuchuk, V. Kladko, Yu. Bacherikov, T. Konstantinova, and L. Khomenkova, *Phys. Stat. Sol. C.*, **11**, 1417 (2014).
18. T. E. Konstantinova, V. V. Tokii, I. A. Danilenko, G. K. Volkova, S. V. Gorban, N. V. Tokii, and D. L. Savina, *Nanosystems, Nanomaterials, Nanotechnologies*, **6**, 1147 (2008).
19. T. E. Konstantinova, A. V. Ragulya, A. S. Doroshkevich, G. K. Volkova, and V. A. Glazunova, *Int. J. Nanotechnology*, **3**, 29 (2006).
20. T. Konstantinova, I. Danilenko, V. Glazunova, G. Volkova, and O. Gorban, *J. Nanoparticle Res.*, **13**, 4015 (2011).
21. M. Anpo, T. Nomura, J. Kondo, K. Domen, K. I. Maruya, and T. Onishi, *Res. Chem. Intermediate*, **13**, 195 (1990).
22. J. S. Lakshmi, I. John Berlin, G. P. Daniel, P. V. Thomas, and K. Joy, *Physica B*, **406**, 3050 (2011).
23. K. Smits, D. Millers, L. Grigorjeva, J. D. Fidelus, and W. Lojkowski, *J. Phys.: Conf. Ser.*, **93**, 012035 (2007).
24. Q. Li, D. Ai, X. Dai, and J. Wang, *Powder Technology*, **137**, 34 (2003).
25. N. Korsunska, M. Baran, A. Zhuk, Yu. Polishchuk, T. Stara, V. Kladko, Yu. Bacherikov, Ye. Venger, T. Konstantinova, and L. Khomenkova, *Mater. Research Express*, **1**, 045011 (2014).
26. H. K. Yueh and B. Cox, *J. Nucl. Mater.*, **323**, 57 (2003).
27. C. Lin, C. Zhang, and J. Lin, *J. Phys. Chem. C*, **111**, 3300 (2007).
28. V. M. Orera, R. I. Merino, Y. Chen, R. Cases, and P. J. Alonso, *Phys. Rev. B*, **42** 9782 (1990).
29. R. I. Merino and V. M. Orera, *Sol. St. Ionics*, **76**, 97 (1995).
30. K. H. Jacob, E. Knozinger, and S. Benfer, *J. Chem. Soc. Faraday Trans.*, **90**, 2969 (1994).
31. M. Bhagwat, A. V. Ramaswamy, A. K. Tyagi, and V. Ramaswamy, *Mater. Res. Bull.*, **38**, 1713 (2003).
32. Y. S. Zhang, L. T. Hu, H. Zhang, J. M. Chen, and W. M. Liu, *J. Mater. Proc. Technol.*, **198**, 191 (2008).
33. Y. Zorenko, T. Voznyak, and R. Turchak, *Acta Phys. Polon. A*, **117**, 199 (2010).
34. M. D. McCluskey and S. J. Jokela, *J. Appl. Phys.* **106**, 071101 (2009).
35. Y. Zhao and G. Horlick, *Spectrochim. Acta. Part B.*, **61**, 674 (2006).
36. A. A. Altynhhikov, L. T. Tsikoza, and V. F. Anufrienko, *J. Structural Chemistry*, **47** 1161 (2006).
37. R. J. Singh, A. Punnoose, J. Mathew, B. P. Maurya, M. Umar, M. I. Haque, and M. I. Phys. *Rev. B.* **49**, 1346 (1994).
38. L. D. Bogomolova, V. A. Gan'shin, V. A. Jachkin, M. E. Kubrinskaya, and V. Z. Petrova, *J. Non-Cryst. Sol.* **45**, 249 (1981).
39. V. F. Anufrienko, R. A. Shutilov, G. A. Zenkovets, V. Yu. Gavrilov, N. T. Vasenin, A. A. Shubin, T. V. Larina, A. V. Zhuzhgov, Z. R. Ismagilov, and V. N. Parmon, *Russian Journal of Inorganic Chemistry*, **57**, 1285 (2012).
40. M. Rashad, M. Rüsing, G. Berth, K. Lischka, and A. Pawlis, *Journal of Nanomaterials*, article ID 714853 (6 pages) (2013).